Available online at www.sciencedirect.com
ScienceDirect
Science and Technology of Advanced Materials 8 (2007) 644–654
SCIENCE AND TECHNOLOGY OF ADVANCED MATERIALS
www.elsevier.com/locate/stam

Relation between microstructure, properties and spark plasma sintering (SPS) parameters of pure ultrafine WC powder

Giovanni Maizza[a], Salvatore Grasso[a], Yoshio Sakka[b,*], Tetsuji Noda[b], Osamu Ohashi[c]

[a]*Department of Materials Science & Chemical Engineering, Politecnico di Torino, Corso Duca Abruzzi 24, I-10129 Turin, Italy*
[b]*National Institute for Materials Science, Ibaraki 305-0047, Japan*
[c]*Graduate School of Science & Technology, Niigata University, Niigata 950-2181, Japan*

Received 12 June 2007; received in revised form 23 August 2007; accepted 10 September 2007
Available online 31 October 2007

Abstract

A combined experimental/numerical methodology is developed to fully consolidate pure ultrafine WC powder under a current-control mode. Three applied currents, 1900, 2100 and 2700 A, and a constant pressure of 20 MPa were employed as process conditions. The developed spark plasma sintering (SPS) finite-element model includes a moving-mesh technique to account for the contact resistance change due to sintering shrinkage and punch sliding. The effects of the heating rate on the microstructure and hardness were investigated in detail along the sample radius from both experimental and modeling points of view. The maximum hardness (2700 HV10) was achieved for a current of 1900 A at the core sample, while the maximum densification was achieved for 2100 and 2700 A. A direct relationship between the compact microstructure and both the sintering temperature and the heating rate was established.

Keywords: Pure WC powder; SPS; Thermoelectric model; Finite element; Current-control mode; Heating rate; Moving mesh; Electric contact resistance

1. Introduction

Pure WC powders are typically sintered in the presence of Co, Fe or Ni in the liquid phase by various techniques. Metallic binders may be introduced to promote WC interparticle bonding and to increase the compact toughness. However, metallic binders usually result in reduced hardness and corrosion/oxidation resistance [1] and enhance grain growth, particularly in conventional liquid-phase sintering due to rapid diffusion in the liquid phase [2]. To promote sintering in conventional methods, several transition-metal carbides, such as Mo_2C and TiC, are usually added as carbide binders [3]. It has been observed, for instance, that when TiC is added to WC–TiC–TaC composites, WC forms a solid solution phase with TiC [4]. In contrast, when carbides such as Mo_2C–TiC–TaC are added to WC, they may cause a decrease in wear resistance and toughness in comparison with WC–Co systems due to carbon segregation at WC–TiC grain boundaries [5]. Undesirable grain growth in conventional WC–Co systems can be reduced using grain growth inhibitors. Kawakami et al. [6] have shown that the effect of grain growth inhibitors is related to their dissolution in the liquid phase, and that their efficiency in grain boundary pinning decreases in the order $VC > CrC_2 > TiC > TaC$.

Pure ultrafine (UF) WC powder has recently attracted an increased interest in the hard-metal industry due to its potential advantages, related to its unique properties suitable for a wide range of advanced applications such as dies for aspherical glass lens forming [7], microdies [8–10] and electrodes for micro-electro-discharge machining. The current demand for UF carbide manufacture is mainly driven by the need for increasing hardness, wear resistance and toughness.

To satisfy these demands, pure UF WC powder is very promising, although it poses severe difficulties such as spontaneous agglomeration, high reactivity, ease of surface contamination and grain coarsening.

UF or nanoscale powders are usually metastable due to their large surface area. It is expected that grain boundary diffusion is predominant in these powders, particularly in

*Corresponding author. Tel.: +81 29 859 2461; fax: +81 29 859 2401.
E-mail address: SAKKA.Yoshio@nims.go.jp (Y. Sakka).

1468-6996/$ - see front matter © 2007 NIMS and Elsevier Ltd. All rights reserved.
doi:10.1016/j.stam.2007.09.002

the early stage of sintering. In addition, WC powder exhibits a high melting point, which severely restricts the choice of sintering techniques that can be used. Thus, the full consolidation of pure UF WC powder, although very useful practically and exciting scientifically, appears to be difficult and energy-consuming, particularly when conducted by conventional methods, such as hot pressing.

An alternative method for sintering pure WC powder is spark plasma sintering (SPS). The primary unique features of the SPS process are its current effects (i.e., not essentially limited to Joule heating) [11] and heating rate, whose effects on densification and microstructure are not yet well understood in detail [11]. On this basis, the effects of the heating rate in the SPS process, which can be greater than 1000 °C/min, cannot be compared with those at 50–80 °C/min in hot pressing.

Using the SPS process, several authors have succeeded in the full consolidation of binderless WC [3,4,12–14]. These authors have carried out SPS experiments under either temperature-control mode [3,4,12–14] or current-control mode [4]. Note that binderless WC powder usually contains a small amount (about 0.2 wt%) of grain growth inhibitors such as VC or Cr_3C_2. In a typical temperature-control mode, a pre-set temperature cycle is programmed and then monitored at a probe point on the die surface, while the SPS machine automatically adjusts the electric potential to fulfill the assigned temperature cycle. In the SPS current-control mode, a constant current intensity is usually applied instead. As a result, a temperature field originates in the system as the complex interplay of electric and thermal phenomena in the bulk and at the contact interfaces between the machine parts, or between the machine parts and the powder compact.

In the SPS process, however, the measured temperature is not directly related to the sintering temperature. The sintering temperature is generally determined by intricate thermoelectrical phenomena in the system in which the contact resistance at the various interfaces plays a crucial role. Therefore, an extensive fundamental understanding of the SPS process is required to control the process and, in turn, the compact microstructure and its properties.

A number of SPS sintering models [15–19] have proposed to improve the fundamental knowledge underlying the SPS process. These models have been mainly designed to predict the temperature and current fields. However, most of them apply to the SPS temperature-control mode and do not include the effects of contact resistance caused by the punch sliding as a result of the compact shrinkage.

The primary purpose of this study is to develop a combined experimental/numerical methodology that will enable the full consolidation of pure UF WC powder by the SPS process and to establish a direct relationship between the compact microstructure and both sintering temperature and heating rate. The experimental strategy is based on SPS experiments conducted under the current-control mode at three specified current values with the same and constant applied pressure. The developed SPS model incorporates a moving finite-element mesh model that takes into account the contact resistance change due to compact shrinkage and punch sliding.

2. Experimental procedure

The employed UF WC powders were supplied by the A.L.M.T. Corp., Japan, and have the commercial name of WC02NR [20]. Powder specifications are as follows: grain size: 0.10–0.14 μm, according to Brunauer, Emmet and Teller (BET) analysis and scanning electron microscopy (SEM), purity: O≦0.60 wt%, free carbon (FC) ≦0.25 wt%, Cr ≦0.007 wt%, Mo, Fe ≦200 ppm, Ca, Si, Ni ≦30 ppm, Al, Cu, Mg, Mn, Sn ≦20 ppm.

Fig. 1 shows a SEM image of the as-received pure WC powder. As can be seen, it consists of both round and elongated WC grains exhibiting severe initial agglomeration. The as-received WC powder is then placed into a hollow graphite cylinder die of 50 mm outer diameter, 20 mm inner diameter and 40 mm height.

The SPS experiments were carried out using a 100 kN SPS-1050 machine (SPS Syntex Inc.). The power source can provide a pulsed or continuous direct current of up to 5000 A. The constitutive elements of the SPS apparatus are shown in Fig. 2.

In general, the SPS apparatus can be operated automatically (i.e., under temperature-control mode) or manually (i.e., under voltage or current-control mode).

In the present work, the current-control mode of the SPS process was selected as an experimental strategy aimed at achieving the full consolidation of pure UF WC powder with minimum grain growth. We used this operating mode since it allowed us to (a) explore the effect of high heating rates, which are believed to be beneficial for sintering UF WC powders and (b) improve the design of SPS sintering experiments with the aid of modeling tools. The use of high

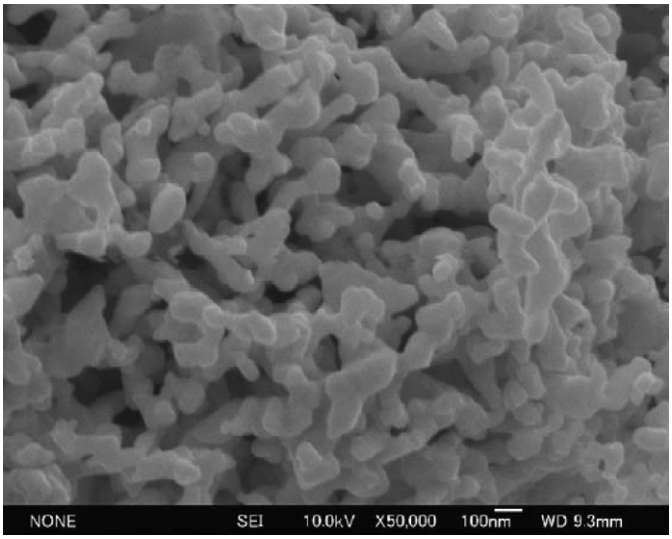

Fig. 1. SEM image of ultrafine WC powder.

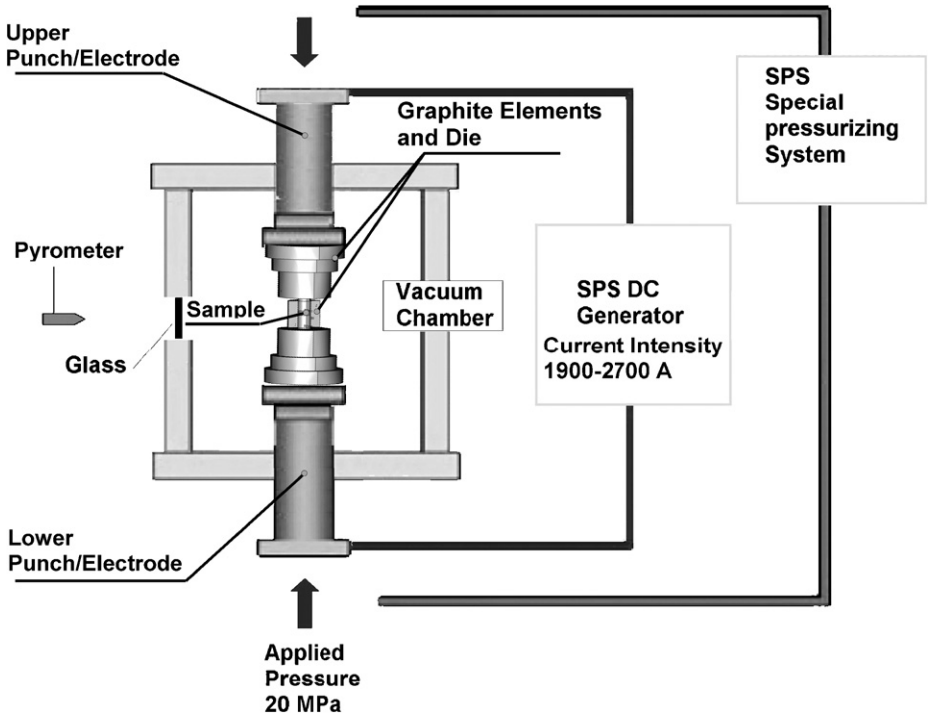

Fig. 2. Schematics of the SPS apparatus.

heating rates implies that the sintering temperature can be reached in a relatively short time, which consequently significantly reduces radiation heat losses. An optical pyrometer that operates above 570 °C is employed to monitor the die surface temperature. Two carbon foils are adopted to avoid interface reactions between the punches and the WC powder. A carbon felt is adopted to minimize radiation losses. The consolidated samples typically have 20 mm diameter and about 2 mm thickness.

All sintering experiments were carried out under vacuum conditions at a constant applied pressure of 20 MPa. Three different DC currents, 1900, 2100 and 2700 A, were investigated. Each current was applied and held constant until the densification rate became negligible. This condition was normally reached when the recorded punch displacement curve approached a steady state. This displacement curve provides a rough measure of the shrinkage due to sintering of the powder compact. The actual shrinkage curve can be used as input data in the SPS simulation model to numerically reproduce the true displacement due to shrinkage during sintering. The procedure for correcting the recorded displacement curve obtained using the model will be described in detail in a subsequent paper [21]. The recorded curve was determined by taking into account the thermal expansion of the graphite parts. This was carried out by experimental (calibration) tests. In the calibration tests, the WC green compact is replaced by a graphite disk in the sintering die.

The relative density was measured by Archimedes' principle. Three points along the disk radius at the midthickness cross section were investigated. These points were taken at the center, 4 and 8 mm from the center, and are denoted hereafter as A, B and C, respectively. The fracture surface microstructure at these points was inspected using a scanning field emission electron microscope (FESEM, JEOL JSM-6500F). The fracture surface was ultrasonically cleaned in acetone. The hardness was measured on diamond-polished cross sections using a Vickers hardness tester (AVK-A Akashi Corporation, Japan) with an applied load of 10 kg and a dwell time of 15 s.

3. SPS model

The SPS process is a multiple-field problem in which the electric, thermal and displacement (i.e., shrinkage) fields are intimately coupled via a material response. This problem is strongly nonlinear since each field interacts with each other and affects the physical properties of the materials. The problem requires the simultaneous numerical solution of each physical field with its own boundary conditions.

The present SPS model is used to numerically reproduce the experiments when the SPS process is operated under the current-control mode. To the best of our knowledge, previous SPS models [15–19] are based on the temperature-control mode.

The overall electric resistance of the SPS system controls the current field and consequently the volumetric heat generation through the Joule effect. This electric resistance includes two contributions: (a) the bulk electric resistance of the machine parts (i.e., punches, die and graphite

elements) and that of the powder compact and (b) the contact resistance at the interfaces. Specifically, the bulk electric resistance is strongly dependent on temperature and volume, the latter being mainly associated with the shrinkage of the powder compact upon sintering. The bulk electric resistance of the powder compact and the contact resistance of the system require special treatment. Here the former resistance is computed by accurately reproducing the transient displacement field inside the compact and that of the upper sliding punch according to the recorded shrinkage of the compact. Thus, only the axial displacements are computed. Using this strategy, the model can reproduce bulk electric resistivity changes in time as the compact densifies.

Regarding the electric contact resistance, we may assume that it is a function of both pressure and the contact surface area between contacting parts, including the sliding parts. In addition, the contact resistance at the die/punch and die/compact interfaces (i.e., the vertical interfaces) includes the relative thermal expansion effects of the punch and die. The electric contact resistance between the graphite elements depends on temperature, whereas that at the punch/compact interfaces (i.e., horizontal interfaces) depends on the temperature and degree of densification of the compact.

The electric and thermal contact resistances were incorporated in the model by designing interface layers whose temperature dependence was determined through an iteration process with the aid of coupled experimental/numerical calibration tests. The temperature dependence was determined for both electric and thermal contact resistances to enhance the predictive capability of the developed model. The unknown parameters were progressively refined through the iteration process by minimizing the deviation between the computed and measured voltage drops and die surface temperature profiles.

Essentially, six calibration tests were designed to determine four contact resistance functions. All tests were conducted under the same applied pressure of 20 MPa, as in actual sintering experiments, and different values of the applied current as follows:

(a) two calibration tests without carbon felt at currents of 1900 and 2100 A with the sample replaced by a graphite test disk having the same volume as the actual WC green compact (i.e., 20 mm diameter, 7 mm height);
(b) two calibration tests with carbon felt at currents of 1900 and 2100 A with the sample replaced by a graphite test disk having the same volume as the actual WC green compact (i.e., 20 mm diameter, 7 mm height);
(c) two calibration tests with carbon felt at currents of 2100 and 2700 A and the UF WC powder compact sample (i.e., 20 mm diameter, 7 mm height), as described in detail in the experimental procedure.

Calibration tests (a) and (b) were used to estimate the horizontal and vertical electric contact resistances between fixed graphite parts (i.e., graphite elements, punches, die and test disk). Additionally, these tests provided useful data on the effect of the carbon felt. Calibration test (c) was used to estimate the electric contact resistances between the WC powder compact and the graphite parts.

First, some trial values [15] were entered in the iteration process and a linear temperature dependence was assumed for both horizontal and vertical resistances. As the number of iterations increased, the estimated functions of the electric contact resistances became increasingly complex and accurate. More details on the calibration procedure will be given in Ref. [21].

As a result of this preliminary study, the electric contact resistance functions along fixed (i.e., horizontal) and sliding (i.e., vertical) surfaces were determined and used in the SPS sintering model.

The electric and thermal fields are described by the standard Poisson and heat conduction equations, respectively. The heat conduction equation includes a Joule heat source term.

To take into account the electric/thermal effects associated with the sliding parts, a moving-mesh technique was incorporated into the SPS model. This technique is particularly suitable for describing the shrinking behavior of UF WC powder compact since it is characterized by a very low initial density. At each instant during the SPS process, the computational finite-element mesh is redrawn according to the actual shrinkage curve. To avoid model complexity, densification evolution is assumed to be spatially uniform and the powder compact is treated as a continuum medium.

The external surfaces of the graphite elements are electrically insulated. A voltage is applied between two water-cooled rams, of which the lower one is grounded. The physical properties of the system such as electric resistivity, thermal conductivity, specific heat, density and thermal expansion coefficient are functions of temperature and residual porosity.

Because the rams, chamber walls and the upper and lower surfaces of the graphite cylinders are water-cooled, a constant temperature of 25 °C was assumed on such element surfaces. Heat convection can be reasonably assumed to be negligible because of the vacuum condition. Radiation heat transfer was assumed to occur between graphite elements and internal chamber walls. The effect of the carbon felt at the die surface was taken into account by introducing a reduction factor of 0.3 for the relative emissivity of graphite (i.e., 0.8 [22]). This reduction factor was estimated in preliminary calibration tests with and without carbon felt [21].

The overall set of coupled partial differential equations describing the SPS process, together with the associate boundary and initial conditions, were solved using a commercially available finite element package [23]. Because of the axial symmetry of the arrangement, only one half of the system domain cross section was required for modeling. Details of the SPS computer model and the

calibration procedure will be provided in a subsequent paper [21].

4. Results and discussion

4.1. Experimental results

Fig. 3 shows the measured die surface temperature and punch shrinkage displacement as a function of time for the three investigated applied currents. Table 1 shows a summary of the measured sintering times, relative density and peak temperature at the die surface. The sintering time is defined as the time from the start of the current flow to when the shrinkage rate becomes negligible. The sintering time at each current is identified in Fig. 3 with a light circle.

Figs. 4–6 show the fracture surfaces as observed by FESEM at points A, B and C for each applied current. By comparing the microstructures along the radius for the applied current of 1900 A, we notice that a slight increase in grain size occurred at points A and B (Figs. 4(a) and (b), respectively) whereas some residual porosity is observed at grain size at point C (Fig. 4(c)). For an applied current of 2100 A, the microstructures at points A and B (Figs. 5(a) and (b), respectively) show more severe anisotropic grain growth than that at point C (Fig. 5(c)). Specifically, the grains at point C are more equiaxial than those at points A and B. In the case of 2700 A (Fig. 6), anisotropic grain growth is even more severe at points A and B than that at the same points for 2100 A. The larger grains at point C are smaller than those at points A and B. Fig. 7 shows the measured hardness at points A, B and C for each applied current.

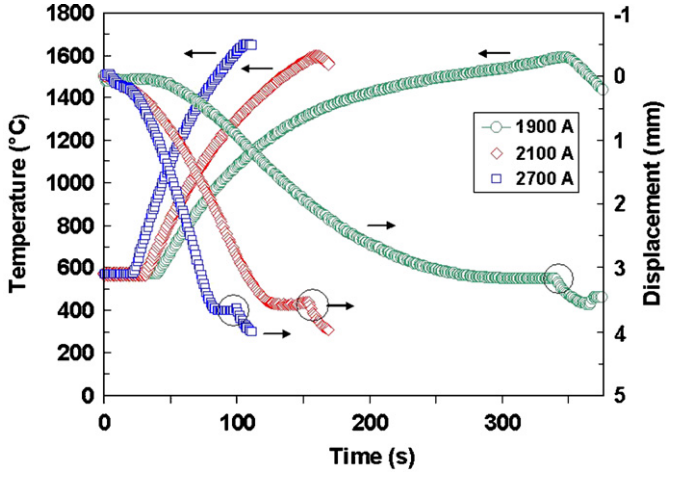

Fig. 3. Measured temperature and displacement as a function of heating time for three applied currents (i.e., 1900, 2100 and 2700 A) during sintering of pure ultrafine WC. The vertical arrows indicate sintering times or steady-state shrinkage rate.

Table 1
Experimental sintering data

	1900 A	2100 A	2700 A
Sintering time (s)	342	156	101
Relative density (%)	97.57	99.48	99.17
Max. temperature (°C)	1585	1580	1616

XRD analysis was used to reveal the formation of W_2C. The XRD spectra did not change with the change in the applied current. Thermogravimetric analysis (not shown) confirms that surface oxides in the initial powders are reduced to W_2C, as also observed by Mizukami et al. [20].

4.2. Modeling results

Since the SPS process does not allow the direct measurement of the sintering temperature, the use of computer modeling is crucial for understanding the process and for controlling the final microstructure and its properties. In the temperature-control mode, the sintering process is completely controlled by the die surface temperature, which does not coincide with the sintering temperature. This makes the analysis and optimization of the SPS process more difficult. In the current-control mode, on the other hand, the applied current directly controls the current flow and, in turn, the sintering process. The computer model is indispensable, first to determine the temperature inside the compact and then to optimize the operating parameters with respect to the desired final microstructure.

Figs. 8 and 9 show (with gray lines) the recorded temperature at the die surface and the experimental applied voltage drop between two rams, respectively. In the same figures, the corresponding numerical results (black lines) are also shown. The best fitting between the experimental and computed values in Figs. 8 and 9 is for the result of the calibration procedure, which allowed the determination of the system contact resistance [21]. As can be seen, the agreement is very satisfactory. Fig. 10 shows the isotherms at the end of the sintering process for each applied current. On increasing the applied current, the sintering time is reduced and the sample temperature increases proportionally. For each applied current, the maximum temperature is at the punch/graphite element interface. By increasing the current intensity, heating becomes increasingly nonuniform. Fig. 11 shows how the moving mesh evolves from the beginning (a) to the end (b) of the sintering process as the powder compact shrinks. The square on the right-hand side of each figure shows the details of the sample discretization mesh before (a) and after (b) the sintering. The high density of the mesh at the interfaces highlights the role of the contact resistance during sintering.

4.3. Discussion of the results

According to the literature it is difficult to understand why the sintering of pure UF WC powders is possible by SPS, whereas it is difficult by conventional hot pressing. We believe that the main reason can be attributed to the heating method and to the effects of the current flow. It has

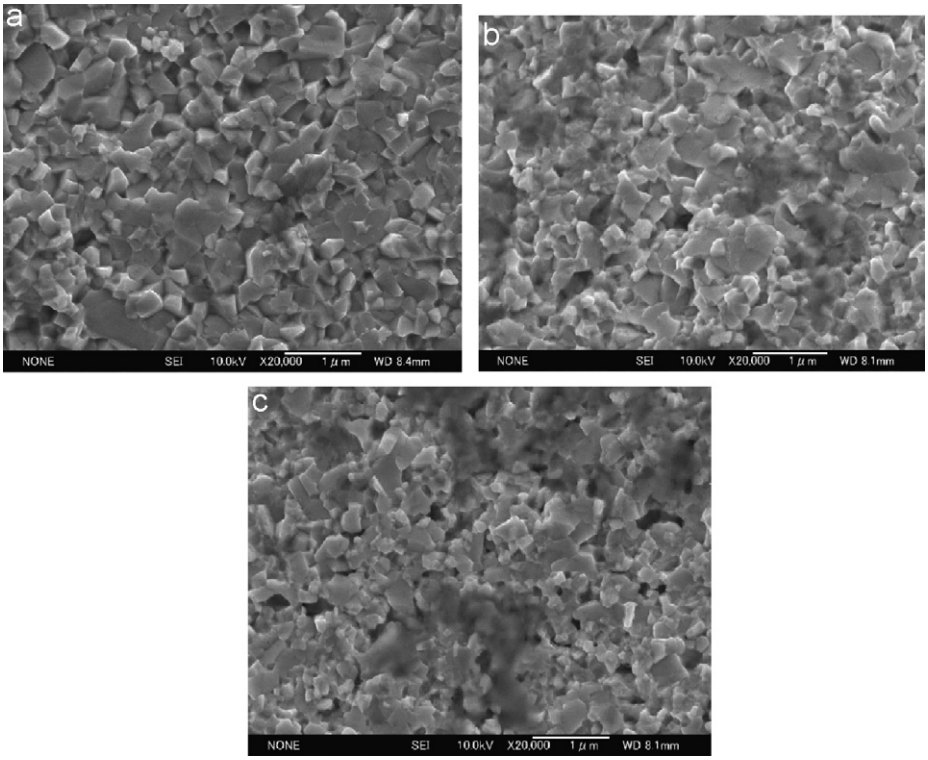

Fig. 4. FESEM fracture surface micrographs of pure ultrafine WC after sintering at 1900 A applied current (a) at the sample center, (b) 4 mm from the center and (c) 8 mm from the center along the radius of midthickness cross section.

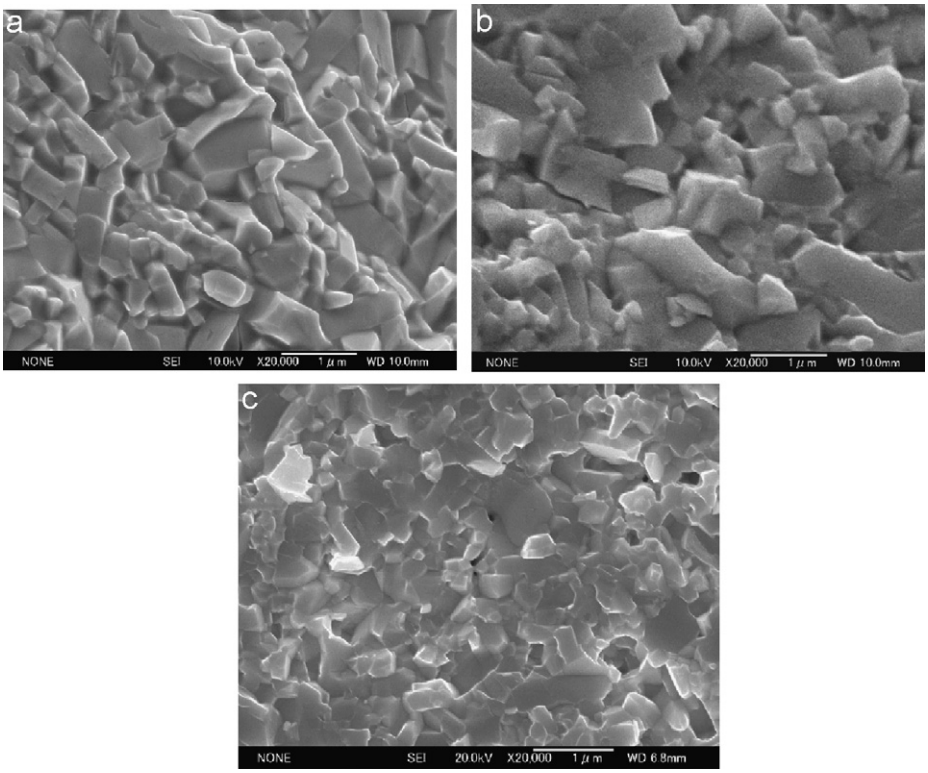

Fig. 5. FESEM fracture surface micrographs of pure ultrafine WC after sintering at 2100 A applied current (a) at the sample center, (b) 4 mm from the center and (c) 8 mm from the center along the radius of midthickness cross section.

been demonstrated that the effect of the current is not limited to Joule heating, but it also plays an important role in oxide film disruption and mass transport [11]. To directly compare the sinterability of SPS and hot pressing, it is necessary to apply the same sintering conditions. The heating rate cannot be assumed to be identical in both

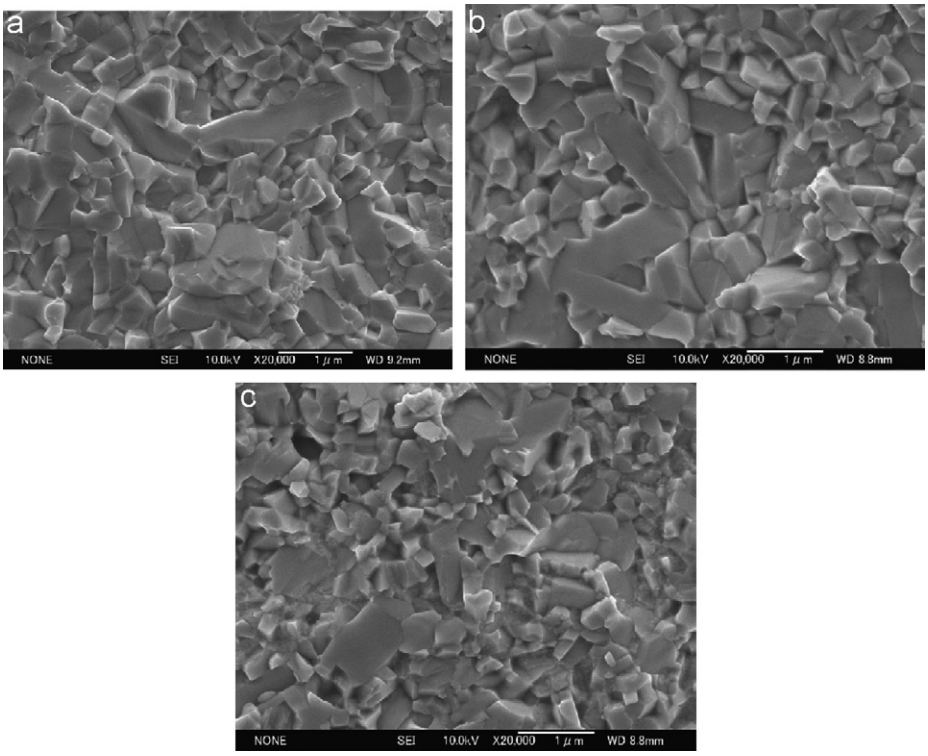

Fig. 6. FESEM fracture surface micrographs of pure ultrafine WC after sintering at 2700 A applied current (a) at the sample center, (b) 4 mm from the center and (c) 8 mm from the center along the radius of midthickness cross section.

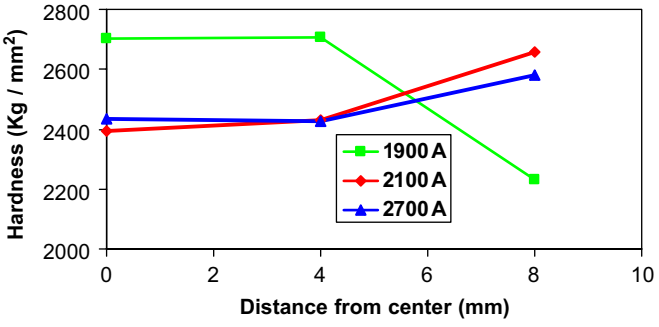

Fig. 7. Measured hardness profiles at points A, B and C along the radial direction of the sample for three applied currents (1900, 2100 and 2700 A).

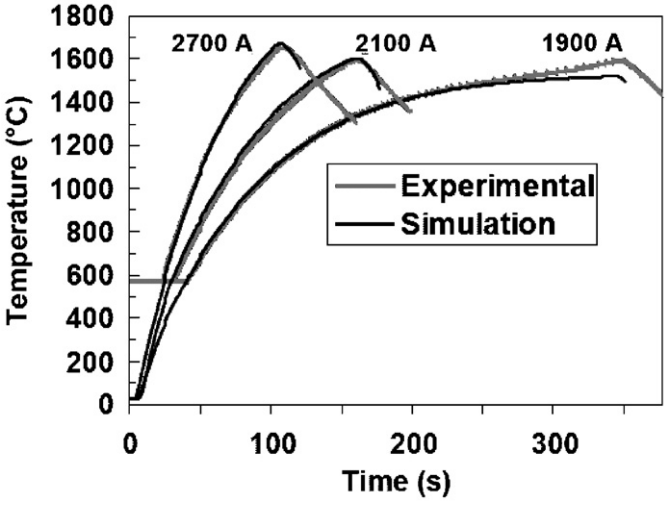

Fig. 8. Comparison of the measured and computed temperatures as a function of time at the die surface for three applied currents (i.e. 1900, 2100 and 2700 A).

cases. In the SPS process, the accurate prediction of the current distribution and heating conditions are crucial steps.

In Fig. 12, it is clearly shown that the heating rate increases with the applied current, and with the increase in current, the sintering time markedly decreases, even if the measured maximum temperature on the die surface is almost the same (see also Table 1). This may imply that the sintering temperature increases as the applied current increases.

Consequently, as shown in Fig. 3, the densification rate increases with the applied current. Kim and co-workers [2,4] found similar sintering behavior using WC–10Co and binderless WC powder under the current-control mode. Kim et al. [2] found a temperature difference of 300 °C between the die surface (at 1500 °C) and the sample/die interface (measured using a thermocouple). Note that although Kim et al. [4] used a similar SPS configuration and the same range of applied currents as those used herein, their densification results differ from those found in this work. However, a fair comparison with such results cannot be established because of the different applied pressure and graphite properties, and the application of

carbon felt. In the current-control mode, pressure is an important parameter that controls heating through the electric resistance of the system [18]. The presence of carbon felt, on the other hand, can also significantly affect the surface temperature, as shown in Fig. 13. These temperature lines are recorded on the die surface using a pyrometer with and without the carbon felt and for an applied current of 2100 A. In this case, a graphite disk of 7 mm height and 2 cm diameter was employed in place of the WC powder.

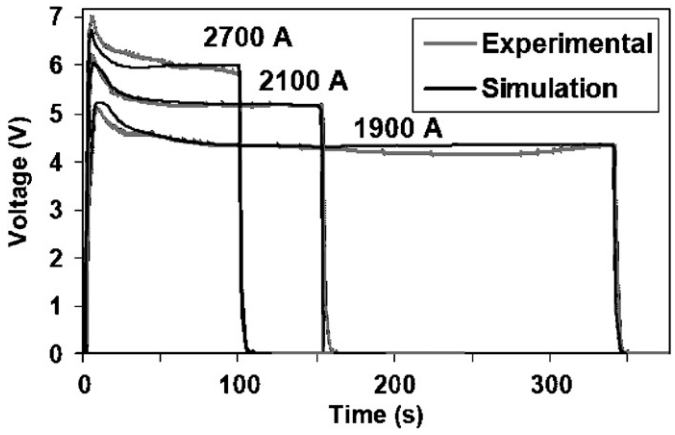

Fig. 9. Comparison of the measured and computed voltage drop between the two rams as a function of time for three applied currents (i.e. 1900, 2100 and 2700 A).

Experimental evidence of a temperature gradient along the radius has also been reported by Abe et al. [24] in the case of metal composites, by Wang et al. [25] for BN and by Sumi et al. [26] for conductive and nonconductive powders. The current distribution (together with radiation heat losses) was attributed to be the main cause of the temperature gradient between the sample and the external die surface [18].

A high heating rate, despite its advantages, may cause inhomogeneous heating of the powder/mold/punch system. As a result, microstructure inhomogeneities and porosity changes may occur along the radial direction.

A comparison of Figs. 4(a), 5(a) and 6(a) shows that the microstructure at point A is strongly dependent on the

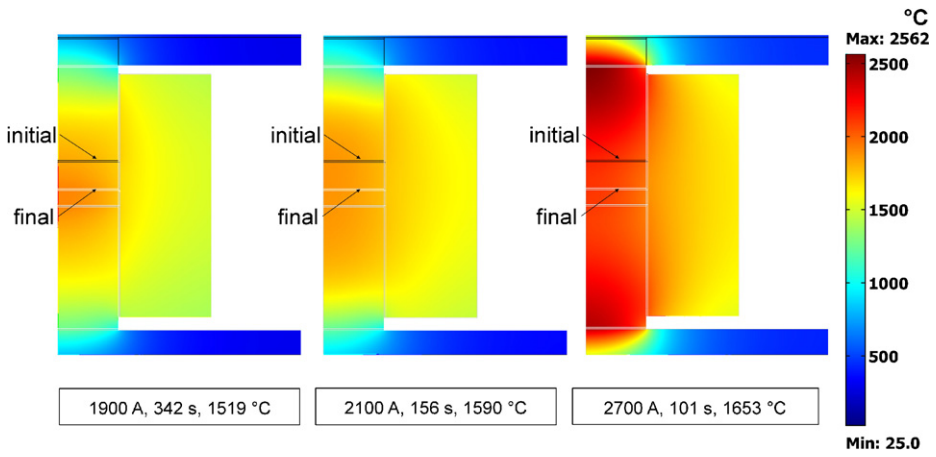

Fig. 10. Temperature distribution inside the punches/die/sample system after sintering before currents switched off for (a) 1900, (b) 2100 and (c) 2700 A. The dark and light lines indicate the initial and final configurations respectively. The computed values of the sintering time and the surface (peak) temperature at the die surface are also given.

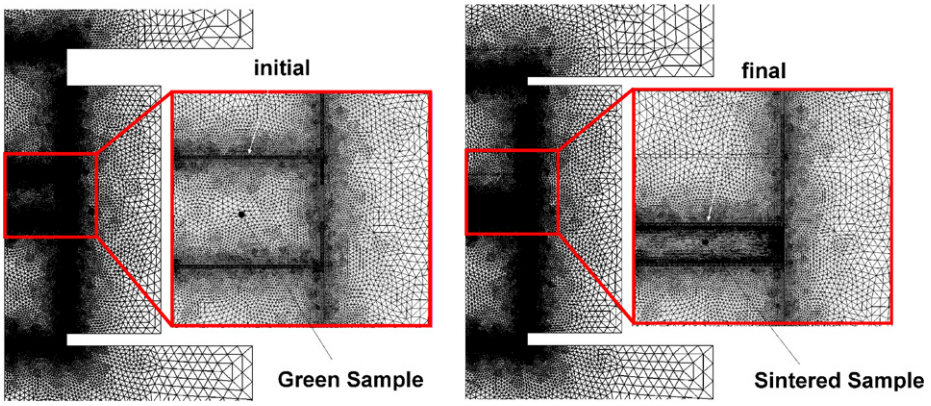

Fig. 11. Finite-element discretization in the punches/die/sample system at the (a) initial and (b) final stage of sintering. The right-hand regions show the details of the sample discretization mesh in both configurations.

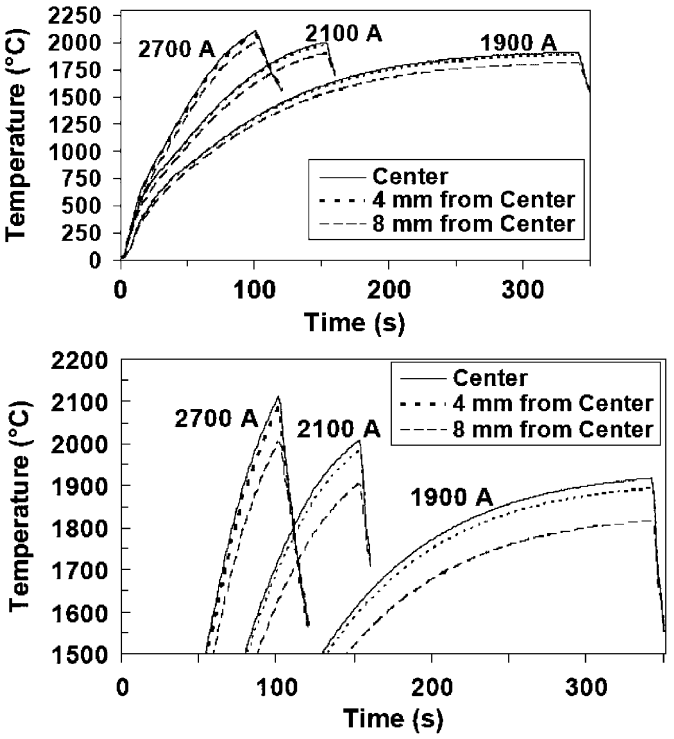

Fig. 12. (a) Computed temperature profiles as function of time for three applied currents (1900, 2100 and 2700 A) at points A, B and C along the radial direction of the sample and (b) enlargement of area between 1500 and 2200 °C.

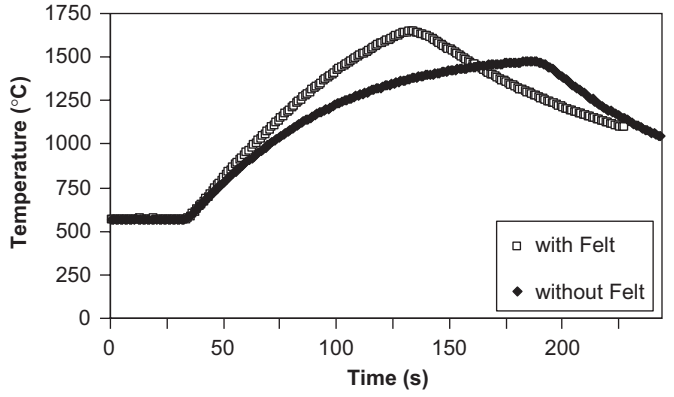

Fig. 13. Measured die surface temperature with and without carbon felt for an applied current of 2100 A as measured from the calibration test using a graphite disk (height 7 mm) instead of the WC powder.

applied current. Some WC grains of up to 2 μm tend to grow, as shown in Fig. 6(a), as the current increases. Shimojima et al. [13], using UF WC powder from the same supplier as that used for this work, and operating in the temperature-control mode, found similar coalescence phenomena, although their powder contained 1 wt% Cr_3C_2 as a grain growth inhibitor. Kim et al. [4], using SPS in the current-control mode and a different WC powder, found that WC grains tended to become a triangular prism shape when the current changed from 2000 to 2800 A. For instance, comparing the case of 2300 A in Ref. [4] and that of 2100 A in this work, the former authors reported a lower sintering temperature and lower density. This discrepancy can be attributed to the use of carbon felt in this work, which limits the radiation losses and affects the surface temperature (see Fig. 13).

The microstructures at point B (Figs. 4(b), 5(b) and 6(b)) exhibit similar features to those at point A for all currents. This consideration is quantitatively supported by hardness measurements (Fig. 7).

The microstructures and hardness at point C (Figs. 4(c), 5(c), 6(c) and 7), however, significantly differ from those at points A and B for each current. Such differences can be primarily attributed to different local sintering temperatures. Thus, accurate knowledge of the sintering temperature inside the sample is of primary importance in understanding the evolution of sintering inside the sample and to tailor the microstructure with respect to the desired proprieties. To achieve this, the relationship between the microstructure and SPS process parameters is required. Because we are not able to experimentally determine the temperature inside the sample, we have to rely on computer modeling provided that the developed model is validated beforehand. In this case, the model has been validated with respect to the die surface temperature and voltage drop, as shown in Figs. 8 and 9. Fig. 12 shows the summary of the computed time–temperature profiles at points A, B and C for each applied current. The computed sintering temperature allows us to define a direct relationship between the sintering temperature, microstructure and hardness as follows. The figure suggests three main interrelated results: (a) the sintering temperature increases with the applied current intensity; (b) the sintering time decreases as the sintering temperature increases; and (c) the heating rate increases monotonically as the sintering temperature increases. These results are in agreement with the experimental evidence in terms of microstructure, hardness, densification rate, surface temperature and voltage drop.

Since the sintering time decreases with the applied current, whereas the maximum die surface temperature is almost the same for each applied current (Table 1), the temperature difference between the compact core and the die surface (Fig. 12) is directly proportional to the applied current. Consequently, grain growth may occur for higher currents.

Table 2 shows the computed maximum temperature at points A, B and C and the measured sintering time for each applied current. As can be seen, temperature decreases from the center to the edge for each applied current. The computed maximum heating temperature is approximately the same at points A and B.

Fig. 4 shows that for a current of 1900 A, grain growth is restricted. The average measured grain size at points A, B and C is as low as 200–250 nm, although Fig. 4(c) (point C) shows some residual porosity. These results are consistent with hardness measurements (Fig. 7). The hardness values at the sample core (i.e., points A and B) compare favorably with those in Refs. [12,13]. Although the sintering

Table 2
Computed maximum temperature (°C) at points A, B, and C for currents of 1900, 2100 and 2700 A

Sample position	1900 A	2100 A	2700 A
A	1917	2009	2099
B	1892	1983	2071
C	1814	1903	1990
Sintering time (s)	342	156	101

conditions considered herein and those in Refs. [12,13] are different from each other, the microstructures at points A and B and those in Refs. [12,13] are similar in terms of the average grain size, being in the range of 0.2–0.5 μm. Such microstructures may have hardness as high as 2700 HV, provided that their full densification is achieved and that the die surface temperature is constant in the range of 1587–1697 °C. A microstructure of 0.2–0.5 μm grain size with a hardness of 2700 HV was obtained in this work at the applied current of 1900 A, the sintering time of 342 s, the measured die surface temperature of 1585 °C and the predicted sintering temperature of 1892 °C.

For applied currents of 2100 and 2700 A, the microstructures at points A and B (Figs. 5(b), (c), 6(b) and (c)) show noticeable grain growth and appear to be inhomogeneous along the radius. Grain growth is significant at the center, whereas it is less pronounced towards the surface (i.e., at point C in Figs. 5(c) and 6(c)). This is also consistent with hardness measurements (Fig. 7). Thus, according to Fig. 7 the hardness change along the radius can be attributed to incomplete densification for the 1900 A current and to the finer microstructure for both 2100 and 2700 A currents. Indeed, the final temperature at point C for the 1900 A current is only 1814 °C, which appears to be insufficient for the full densification of pure WC.

In contrast, for the 2100 and 2700 A currents, the maximum temperatures are sufficiently high to achieve full densification. Since full densification is achieved at these two currents, the approximately equal hardness observed at points A and B can be attributed to the similar average grain size.

The difference in hardness at point C for currents of 2100 and 2700 A is due to the higher temperature for the latter case. Also, the points C and B at 2100 and 2700 A, respectively, exhibit different hardnesses but approximately the same maximum temperature (i.e., 1983 and 1990 °C, respectively). This can be attributed to both different heating rates and different heating times above 1900 °C, which can be considered to be a critical temperature above which grain growth becomes significant.

Thus, all the above considerations confirm that microstructure (or hardness) inhomogeneities along the radius occur in a WC compact when different currents are applied. Microstructure or hardness inhomogeneities along the radius are directly related to local temperature, heating rate and heating time above 1900 °C. For all applied currents, the temperature inside the (conductive) WC compact increases from the surface to the center, as also reported by Sumi et al. [26] for conductive powders. These authors have also experimentally found opposite behavior in (insulating) alumina powder. Wang et al. [27] showed that hardness decreases from the surface to the center in the case of alumina, and explained this phenomenon by considering that the rate of densification greatly exceeded the rate of heat transfer.

5. Conclusions

Pure UF WC powder has been fully consolidated by the SPS process under a current-control mode and three different applied currents.

A suitable combined experimental/numerical methodology allowed us to establish a direct relationship between the compact microstructure and hardness, and the computed sintering temperature and the heating rate.

The contact electric resistance at the die/sample and die/punch interfaces was found to be an important factor in the SPS process since it significantly affects the heat generation and its distribution inside the graphite parts and the compact. This factor makes the SPS system very sensitive to current intensity.

For each applied current, nonhomogeneous densification and a nonhomogeneous microstructure along the radius were observed. The densification behavior together with the microstructure analysis using the developed model showed that the temperature difference between the die surface and the core sample is directly proportional to the applied current. This can be attributed to both different heating rates and different heating times above 1900 °C, which can be considered to be a critical temperature above which grain growth in UF WC becomes significant.

The current-control mode, when used in combination with computer modeling, provides an effective means of systematically designing experiments and exploring the potential of SPS, particularly for the achievement of ultrafine microstructures.

References

[1] H. Suzuki, Cemented Carbide and Sintered Hard Materials, Maruzen, Tokyo, 1986, p. 272.
[2] H.-C. Kim, I.-J. Shon, J.-K. Yoon, J.-M. Doh, Int. J. Refractory Met. Hard Mater. 25 (2007) 46.
[3] S.I. Cha, S.H. Hong, Mater. Sci. Eng. A 356 (2003) 381.
[4] H.-C. Kim, I.-J. Shon, J.E. Garay, Z.A. Munir, J. Refractory Met. Hard Mater. 22 (2004) 257.
[5] H. Engqvist, G.A. Botton, N. Axen, S. Hogmark, J. Am. Ceram. Soc. 83 (2000) 2491.
[6] M. Kawakami, O. Terada, K. Hayashi, J. Jpn. Soc. Powder Powder Metall. 53 (2006) 166.
[7] A.Y. Yi, A. Jain, J. Am. Ceram. Soc. 88 (2005) 579.
[8] K. Hayashi, J. Jpn. Soc. Powder Powder Metall. 53 (2005) 151.
[9] W. Choi, J. Lee, W. Kim, B. Min, J. Micromech. Microeng. 14 (2004) 1519.

[10] S. Sano, M. Nishijima, Y. Maejima, J. Jpn. Soc. Powder Powder Metall. 53 (2005) 177.
[11] Z.A. Munir, U. Anselmi-Tamburini, M. Ohynagi, J. Mater. Sci. 41 (2006) 763.
[12] B. Huang, L.D. Chen, S.Q. Bai, Scr. Mater. 54 (2006) 441.
[13] K. Shimojima, H. Hosokawa, M. Mabuchi, M. Kawakami, S. Sano, O. Terada, N. Asada, Y. Yamamoto, J. Jpn. Soc. Powder Powder Metall. 50 (2003) 844.
[14] H. Kim, D. Choi, J. Kim, Y. Kwon, H. Kwon, E. Baek, in: Seventh Korea–Russia International Symposium on Science and Technology (KORUS 2003).
[15] A. Zavaliangos, J. Zhang, M. Krammer, J.R. Groza, Mater. Sci. Eng. A 379 (2004) 218.
[16] B. McWilliams, A. Zavaliangos, K.C. Cho, R.J. Dowding, JOM (2006) 67.
[17] J. Zhang, A. Zavaliangos, Discrete element simulation of transient thermo electrical phenomena in particulate system, in: S. Sen, M.L. Hunt, A.J. Hurd (Eds.), MRS Proceedings., vol. 759, MRS Fall Meeting, Boston, 2002.
[18] U. Anselmi-Tamburini, S. Gennari, J.E. Garay, Z.A. Munir, Mater. Sci. Eng. A 394 (2005) 139.
[19] U. Anselmi-Tamburini, J.E. Garay, Z.A. Munir, Mater. Sci. Eng. A 407 (2005) 24.
[20] M. Mizukami, Y. Yamamoto, N. Asada, A. Matsutomo, J. Jpn. Soc. Powder Powder Metall. 53 (2005) 154.
[21] G. Maizza, S. Grasso, Y. Sakka, Moving finite element mesh model for aiding spark plasma sintering (SPS) in current control mode of pure ultrafine WC powder, PacRim 7, Symposium on Spark Plasma Sintering (SPS), Shanghai, November 11–14, 2007, to be submitted.
[22] A.I. Savvatimskiy, Carbon 43 (2005) 1115.
[23] Comsol Multiphysics©, AC/DC Module, User Guide 3.3, August 2006.
[24] T. Abe, H. Hashimoto, Y.H. Park, T.Y. Um, Z.M. Sun, in: R.E. Green (Ed.), Nondestructive Characterization of Materials, vol. VIII, Plenum Press, New York, 1998, p. 251.
[25] Y.C. Wang, Z.Y. Fu, W.M. Wang, Key Eng. Mater. 249 (2003) 471.
[26] S. Sumi, Y. Mizutani, M. Yonega, J. Jpn. Soc. Powder Powder Metall. 45 (1997) 1.
[27] S.W. Wang, L.D. Chen, T. Hirai, J. Mater. Sci. Lett. 18 (1999) 1119.